Joint Estimation and Planar Affine Formation Control With Displacement Measurements

Qingkai Yang, *Member, IEEE*, Xiaozhen Zhang, Hao Fang, *Member, IEEE*, Ming Cao, *Fellow, IEEE*, and Jie Chen, *Fellow, IEEE*

***Abstract*— This article investigates the problem of planar affine formation maneuver control with a matrix-valued formation shape variation parameter. The matrix representation renders full degree of freedom (DOF) motion associated with linear mappings in the context of affine transformation. Unlike the typical leader–follower setup, where all the leaders know the prescribed formation information, only a portion of leaders are informed of the matrix parameter in this article. To achieve affine formation stabilization, two types of distributed estimators are developed for the remaining leaders to infer constant and dynamic matrix parameters, utilizing only local displacement measurements. Then, we establish a joint estimation and cooperative control framework, generating corresponding formation shape changes in consistent with the matrix parameter. The system stability and precise estimation convergence are verified via both rigorous theoretical analyses and simulations with large-scale swarms. Finally, experiments conducted on the Crazyflie robots also validate the effectiveness and practicality of the proposed control approach.**

***Index Terms*— Affine formation, formation control, multiagent systems, parameter estimation.**

I. Introduction

FORMATION control has been attracting extended attentions as it provides us with a straightforward framework to reveal and develop the cooperative mechanisms of multiple autonomous agents [1]. The realization of diverse formation patterns can be established based on a range of theories, such as consensus control [2], graph rigidity [3], [4], optimal control [5], and differential game [6], to name a few. From the perspective of practical applications in various fields, it is recognized both in industry and academia that the feasibility and flexibility are essential for the formation system to adapt to the changes and constraints in the ambient working space (e.g., unforeseen disturbances and cyberattacks). To this end, there has been an increasing focus on affine formation control in recent years due to its superiorities in scalability and high degree of freedom (DOF) with respect to collective motions.

Affine formation control is closely related to affine transformation/image, under which the overall formation shape changes according to the embedded transformation matrix. In [7], the necessary and sufficient conditions for the realizability and stabilizability of an affine formation over undirected and directed graphs are given, laying the graphical foundation for the later research on controller design. In [8], the concept of affine localizability is put forward, bridging the gap between the graphical conditions and affine formation maneuver control. Within the proposed hierarchical leader–follower structure, it is only required to control the followers based on the intrinsic stresses. An extension to high-order systems is discussed in [9], where control laws for followers are provided implementing trajectory tracking to leaders. Following a similar control scheme, fully distributed control laws are designed for the general linear-time invariant system with uncertainties [10]. It is proved that the leader–follower structure also applies to high-order systems by employing the back-stepping method [11]. To solve the problem of global stabilization of rigid formations, a two-step method, first converging to the affine space and then stabilizing at one specific formation, is proposed using the sliding mode control and descent gradient control [12]. Besides the feasibility analysis, in [13], it is shown that the formation will converge to a steady-state distorted shape when the sensors have different scale factors and misalignments but with almost perfect sensing. When taking the obstacles into consideration, a feasible path using the A^* search method is first constructed for leaders, based on which the continuum deformation of the whole group is then determined [14] to ensure collision-free. For improving the system performance, the historical velocity command is applied in affine formation controller [15], attaining the explicit relationship between the delay parameter and ultimate bounds of tracking errors.

In task-oriented formation control applications, it is noticed that the real working conditions are far from ideal. For example, agents might suffer from communication constraints for security reasons [16]. In these circumstances, parameter estimation via limited available measurements is essential for

Manuscript received 28 November 2023; revised 16 May 2024; accepted 9 August 2024. This work was supported in part by NSFC under Grant 62373048, Grant 62133002, and Grant 62088101; in part by the National Key Research and Development Program of China under Grant 2022YFB4702000 and Grant 2022YFA1004703; in part by the Fundamental Research Funds for the Central Universities; and in part by Shanghai Municipal Science and Technology Major Project under Grant 2021SHZDZX0100. Recommended by Associate Editor K. Berntorp. *(Corresponding author: Hao Fang.)*

Qingkai Yang, Xiaozhen Zhang, and Hao Fang are with the National Key Laboratory of Autonomous Intelligent Unmanned Systems (KAIUS), School of Automation, Beijing Institute of Technology, Beijing 100081, China (e-mail: qingkai.yang@bit.edu.cn; jiaozhen@mail.nwpu.edu.cn; fangh@bit.edu.cn).

Ming Cao is with the Institute of Engineering and Technology, University of Groningen, 9747 AG Groningen, The Netherlands (e-mail: ming.cao@rug.nl).

Jie Chen is with the Department of Control Science and Engineering, Tongji University, Shanghai 201804, China (e-mail: chenjie@bit.edu.cn).

Digital Object Identifier 10.1109/TCST.2024.3449008

the accomplishment of the prescribed control task. In [17], the projection operator is used to infer the scaling parameter under the so-called monitoring graph. Relying on the relative position measurements with respect to neighbors, Lee and Ahn [18] design a strategy to estimate the global orientation, with which the formation can be stabilized even when the local frames are misaligned. For affine formation maneuver control in $\mathbb{R}^d$, it is generally required at least $d+1$ agents having the knowledge of formation transformation parameter [8]. We call it *minimal realization* in the sense of the number of actively controlled agents. In the case of insufficient informed agents, estimation-based control strategies are proposed in [19] and [20]. Under the mildest assumption that only one agent knows the desired formation scaling parameter, Yang et al. [19] develop the scheme of integrated estimator controller for other d agents, and other agents follow the nominal stress-matrix-based interaction rules. A step further, the mixed rotation-scaling transformations are considered in [20], where the sufficient conditions for the stability of the integrated control framework are given based on cyclic small-gain theorems.

In this article, we consider planar affine formation maneuver control, aiming to enhance the flexibility of shape morphing through the utilization of matrix formation parameters. However, one challenge arises from the insufficient number of informed leaders, which fails to meet the minimum requirement for successful realization. Moreover, unaware agents can only rely on local sensing to coordinate their actions, intensifying the difficulty in achieving global collective behavior. As the displacement changes are affected by the combined influence of multiple components, it becomes unfeasible to separate and identify the specific influence of each individual parameter from the unified measurement.

Specifically, two scenarios will be discussed, i.e., the formation maneuver is guided by constant and time-varying matrices, respectively. Correspondingly, we propose two types of estimators by invoking the descent gradient method and the internal model-like scheme. Concurrently, the agents are actuated based on the current state of the estimators and the underlying stress matrix. The idea behind the joint estimation and control is that the unaware agents can finally perceive the real values of the unknown matrix in a heuristic way through the persistent correction from informed agents on their local displacements.

In summary, this article presents the following primary contributions and advantages.

1) The proposed formation maneuver control method enables more versatile formation patterns than [4], [13], [17], and [21], where limited types of formation transformations are allowed, such as scaling and rotation. In spatially constrained environments, such as obstacle-dense field scenarios, it is generally preferable to variously alter the formations of the multirobot system to adapt to the environmental changes. Toward this end, the proposed method can achieve full DOF affine formation shape transformation. From this perspective, the aforementioned results [4], [13], [17], [21] can be seen as special cases of this article.
2) Instead of estimating a single parameter [17], [19], [21], this article addresses a more complex estimation problem. For the case of single-parameter estimation, the changes in relative positions exhibit the unique mapping relationship with the specific parameter studied in [17], [19], and [21], while elements of the matrix parameter in this article are intrinsically coupled in terms of the measured displacement changes. Consequently, it is challenging to identify the relationship between displacement measurements and unknown parameters in a componentwise manner.
3) The proposed estimation-based affine formation control framework requires less informed leaders than [8] and [11], and can effectively handle both constant and time-varying matrix parameters, as opposed to only considering constant parameters [19], [20].
4) The proposed joint estimation and control framework resolve the excitation conflict in the sense that the precise estimation requires rich displacement changes [22], [23], while formation control drives agents to relatively stable states.
5) To the best of authors' knowledge, it is the first time to verify the effectiveness of the affine formation control method in simulations with large-scale swarms. The results show remarkable superiority in maneuvering the overall formation with only two informed leaders.

This article is organized as follows. Section II provides an introduction to the background of graph theory and affine formation maneuver control. In Section III, a comprehensive solution for formation maneuver control is presented, specifically focusing on scenarios where the matrix parameter is constant. Section IV presents an extensive study on the combined estimation and control scheme tailored to address the challenges posed by time-varying matrix parameters. To demonstrate the effectiveness of the proposed control schemes, Section V showcases their application through simulation and practical implementation on a team of Crazyflie robots. Lastly, concluding remarks are provided in Section VI.

II. Preliminaries

A. Notations

Given two matrices $A \in \mathbb{R}^{m\times n}$ and $B \in \mathbb{R}^{p\times q}$, there holds $A\otimes B \in \mathbb{R}^{mp\times nq}$, where the operator $\otimes$ denotes the Kronecker product. $\mathbf{1}_n \in \mathbb{R}^n$ represents the column vector with all 1s. Similarly, we define $\mathbf{0}_n = [0,\ldots,0]^{\mathrm{T}}$. For a given vector x, we denote by $\|x\|$ as its Euclidean norm. diag $(x_1, x_2, \ldots)$ denotes a diagonal matrix. We use $\lambda_{\max}(X)$ [respectively, $\lambda_{\min}(X)$] to denote the largest (respectively, smallest) eigenvalue of a real symmetric matrix X in any dimension. Given two real symmetric matrices X and Y with the same dimension, $X \succ Y$ means $X-Y$ is positive definite. On the contrary, $X \prec Y$ means $X-Y$ is negative definite.

B. Graph Theory

The team agents and their interaction relationships can be mapped into the graph $\mathcal{G}(\mathcal{V},\mathcal{E})$. The node set $\mathcal{V} = \{1,2,\ldots,n\}$ represents all the agents, and there would be an

edge (i, j) in the set $\mathcal{E}$ if agents i and j have interactions with each other. In this article, the graph is assumed to be simple and undirected, i.e., the existence of (i, j) implies the mutual neighboring relationship between agents i and j. By simple, we mean there is no self-loop and multiple edges in the graph. For each agent i, its neighbor set is defined as $\mathcal{N}_i = \{j|(i, j) \in \mathcal{E}\}$. The neighboring relationship can also be mathematically expressed by the adjacency matrix $\mathcal{A} \in \mathbb{R}^{n\times n}$, whose (i, j)th position is set to be 1 only when agents i and j are neighbors. Note that the adjacency matrix is a binary matrix that only represents the existence of the connection between pairwise agents. The Laplacian matrix $L = [l_{ij}] \in \mathbb{R}^{n\times n}$ is defined by

$$l_{ij} = \begin{cases} -[\mathcal{A}]_{ij}, & i \neq j \\ \sum_{k\in\mathcal{N}_i} [\mathcal{A}]_{ik}, & i = j. \end{cases} \tag{1}$$

Now we will introduce the concept of *universally rigid*. Two related concepts of rigidity are first given for illustration [7]. Consider two frameworks denoted as $(\mathcal{G}, p)$ and $(\mathcal{G}, q)$, where $\mathcal{G}$ represents the graph with two configurations $p = [p_1, \ldots, p_n]^{\mathrm{T}}$ and $q = [q_1, \ldots, q_n]^{\mathrm{T}}$. These two frameworks are deemed *equivalent* if the distances between connected nodes are the same, expressed as

$$\|p_i - p_j\| = \|q_i - q_j\| \quad \forall (i, j) \in \mathcal{E}.$$

More rigorously, they are referred to as *congruent* if the distances between every pair of nodes are identical, given by

$$\|p_i - p_j\| = \|q_i - q_j\| \quad \forall i, j \in \mathcal{V}.$$

A framework $(\mathcal{G}, q)$ in $\mathbb{R}^d$ is characterized as *globally rigid* if, for any configuration p in $\mathbb{R}^d$, the two frameworks $(\mathcal{G}, q)$ and $(\mathcal{G}, p)$ are congruent as long as they are equivalent.

A framework in $\mathbb{R}^d$ is called universally rigid if it is globally rigid in any $\mathbb{R}^{\bar{d}}$ with $\bar{d} \geq d$.

C. Affine Formation Maneuver Control

The affine formation control approach utilizes the leader–follower control structure, where $\mathcal{V}_l$ and $\mathcal{V}_f$ represent the leader and follower sets, respectively. In the context of affine formation control, each edge (i, j) is assigned a weight $\omega_{ij} \in \mathbb{R}$, called stress, which can be either positive or negative. The stress matrix $\Omega \in \mathbb{R}^{n\times n}$ is defined by

$$[\Omega]_{ij} = \begin{cases} \sum_{j\in\mathcal{N}_i} \omega_{ij}, & i = j \\ -\omega_{ij}, & i \neq j. \end{cases} \tag{2}$$

Lemma 1 [7], [24]: If the framework $(\mathcal{G}, q)$ is *universally rigid* in $\mathbb{R}^d$, then the stress matrix Ω is positive semi-definite with $rank(\Omega) = n - d - 1$, and it holds

$$\sum_{j\in\mathcal{N}_i} \omega_{ij} (q_i - q_j) = \mathbf{0}. \tag{3}$$

It is remarked that such a stress matrix can be computed by singular value decomposition (SVD) [8, Sec. VII.A], [25, Algorithm 1] or topological optimization [26].

Prior to giving the problem, we first introduce the basic concepts of affine transformation. Given a configuration $q^* \in \mathbb{R}^{nd}$, the affine transformation of q^* is defined by

$$\mathcal{T}(q^*) = \Big\{ q = \left[\ldots, q_i^{\mathrm{T}}, \ldots\right]^{\mathrm{T}} : q_i = Aq_i^* + b \\ A \in \mathbb{R}^{d\times d}, b \in \mathbb{R}^d, i \in \mathcal{V} \Big\}. \tag{4}$$

where A is called the *linear transformation matrix*, b is the *translational vector*, and q denotes the *target formation*. The objective of the affine formation maneuver control is to shift agents to reach the target formation.

The following Lemma introduces the unique mapping relationship between leaders and followers.

Lemma 2 [8]: For a given framework $(\mathcal{G}, q^*)$ in $\mathbb{R}^d$, if $\{q_i^*\}_{i\in\mathcal{V}_l}$ affinely span $\mathbb{R}^d$, q_f can be uniquely determined by q_l, for any $[q_l^{\mathrm{T}}, p_f^{\mathrm{T}}]^{\mathrm{T}} \in \mathcal{T}(q^*)$, where q_l and q_f are the target formations of leaders and followers, respectively.

D. Problem Statement

This article considers the planar leader–follower formation problem with a group of n agents. Each agent is modeled by the single-integrator dynamics

$$\dot{q}_i = u_i \tag{5}$$

where $q_i \in \mathbb{R}^2$ represents the planar Cartesian coordinate, and $u_i \in \mathbb{R}^2$ is the velocity commands to agent i. That means the position of agent i can be directly controlled via u_i. To provide a formal description of the nominal configuration, we introduce the following assumption.

Assumption 1: The nominal framework $(\mathcal{G}, q^*)$ is universally rigid, and $\{q_i^*\}_{i\in\mathcal{V}_l}$ affinely span $\mathbb{R}^2$.

In view of Lemma 2, it is noted that Assumption 1 is a sufficient condition for determining followers' formation by leaders. In Assumption 1, at least three leaders are required in order to meet $\{q_i^*\}_{i\in\mathcal{V}_l}$ affinely span $\mathbb{R}^2$. Consequently, the leader set is chosen as $\mathcal{V}_l = \{1, 2, 3\}$ with the corresponding subgraph $\mathcal{G}_l$. Correspondingly, the sets $\mathcal{N}_i^l$, $i = 1, 2, 3$ denote the neighboring relationship in $\mathcal{G}_l$. Other follower agents are grouped in the set $\mathcal{V}_f$, i.e., $\mathcal{V}_f = \{4, \ldots, n\}$.

Generally, to activate the cascade leader–follower control in affine formation control [8], [27], all leaders are informed of the desired formation, e.g., the linear transformation matrix A. However, this article considered a milder condition that only two of the leaders (agents 1 and 2) know A, as shown in Fig. 1. The rest of the agents are only allowed to use their local displacement measurements to steer themselves to form the desired formation determined by the nominal configuration q^* and the matrix A. The control objective can be mathematically formulated as

$$\lim_{t\to\infty} r_{ij}(t) = A(t) \cdot r_{ij}^* \quad \forall i, j \in \mathcal{V}. \tag{6}$$

where $r_{ij} = q_i - q_j$ and $r_{ij}^* = q_i^* - q_j^*$. We will design estimators for agent 3 to acquire the information of $A(t)$ in both cases of constant and time-varying matrices. Accordingly, the control strategies will also be presented, respectively.

Remark 1: Given a nominal configuration q^*, the realization of the control objective (6) implies that the formation

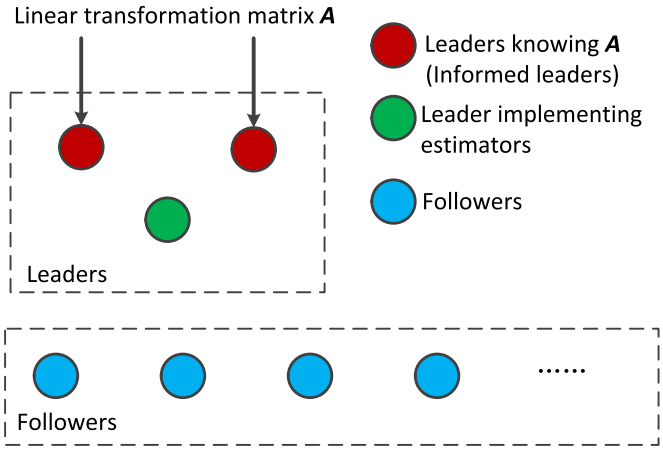

Fig. 1. Schematic of the configuration of formation parameter A.

shape can be regulated by the linear transformation matrix A without the consideration of the translational motion. This coincides with the fact that only relative position measurements are allowed to be used, and thus, the absolute location of the whole formation cannot be determined. It is also worth noting that q^* is provided as the virtual reference to assist formation variations, which does not serve as the desired absolute positions.

Remark 2: The estimation-based methods in this article can also be extended to d-dimensional space, where $d+1$ is the minimal number of leaders that affinely span $\mathbb{R}^d$ required by Lemma 2. Consequently, in a d-dimensional space, d agents know the affine transformation matrix A, and one leader is equipped with estimators. As a result, more relative displacement measurements among leaders should be conducted.

III. Affine Formation Maneuver Control Under Constant Matrix A

Before moving on, we first introduce two definitions to facilitate the following analyses.

Definition 1: Let C be an $n \times m$ matrix. The vectorization of C, denoted by $\mathrm{vec}(C)$, is the nm-dimensional vector obtained by concatenating the columns of the matrix C, defined as

$$\mathrm{vec}\,(C) = \left[c_{\cdot 1}^{\mathrm{T}}, c_{\cdot 2}^{\mathrm{T}}, \ldots, c_{\cdot m}^{\mathrm{T}}\right]^{\mathrm{T}}$$

where $c_{\cdot i} \in \mathbb{R}^n$ represents the ith column of the matrix C.

Definition 2: Given any vector $x = [x_1, \ldots, x_d]^{\mathrm{T}} \in \mathbb{R}^d$, the operation, denoted by $\mathrm{Mat}(x)$, performed over the vector x results in a $d \times d^2$ matrix defined by

$$\mathrm{Mat}\,(x) = x^{\mathrm{T}} \otimes I_d.$$

With these two definitions, one has the following conclusion.

Proposition 1: Given any matrix $C \in \mathbb{R}^{d\times d}$ and vector $v_i \in \mathbb{R}^d$, $i = 1, \ldots, n$, there holds

$$\alpha_1 C v_1 + \cdots + \alpha_n C v_n = \left(\mathbf{1}_n^{\mathrm{T}} \otimes I_d\right) \begin{bmatrix} \alpha_1 \mathrm{Mat}\,(v_1) \\ \vdots \\ \alpha_n \mathrm{Mat}\,(v_n) \end{bmatrix} \mathrm{vec}\,(C)$$

where $\alpha_i, i = 1, \ldots, n$, is an arbitrary constant.

Proof: From Definitions 1 and 2 and basic multiplication principles of matrices, we immediately have

$$Cx = \mathrm{Mat}\,(x)\,\mathrm{vec}\,(C) \quad \forall x \in \mathbb{R}^d.$$

Consequently, one has

$$\begin{aligned} &\alpha_1 C v_1 + \cdots + \alpha_n C v_n \\ &\quad = \alpha_1 \mathrm{Mat}\,(v_1)\,\mathrm{vec}\,(C) + \cdots + \alpha_n \mathrm{Mat}\,(v_n)\,\mathrm{vec}\,(C) \\ &\quad = (\alpha_1 \mathrm{Mat}\,(v_1) + \cdots + \alpha_n \mathrm{Mat}\,(v_n))\,\mathrm{vec}\,(C) \\ &\quad = \left(\mathbf{1}_n^{\mathrm{T}} \otimes I_d\right) \begin{bmatrix} \mathrm{Mat}\,(v_1) \\ \vdots \\ \mathrm{Mat}\,(v_n) \end{bmatrix} \mathrm{vec}\,(C) \end{aligned}$$

where the last equality holds by directly taking the multiplication operation of the first two terms in the last line. This completes the proof. □

The distributed control laws are given by

$$u_i = -k_3 \sum_{j\in\mathcal{N}_i} \omega_{ij} r_{ij} - k_1 \sum_{j\in\mathcal{N}_i^l} \left(r_{ij} - \bar{A} r_{ij}^*\right), \quad i \in \mathcal{V}_l \tag{7a}$$

$$u_i = -k_3 \sum_{j\in\mathcal{N}_i} \omega_{ij} r_{ij}, \quad i \in \mathcal{V}_f \tag{7b}$$

where

$$\bar{A} = \begin{cases} A, & i = 1, 2 \\ \hat{A}, & i = 3 \end{cases}$$

with $\hat{A}$ the estimation of the linear transformation matrix $A \in \mathbb{R}^{2\times 2}$. $\mathcal{N}_i^l$ and $\mathcal{N}_i$ denote the neighbor sets in graphs $\mathcal{G}_l$ and $\mathcal{G}$, respectively. k_3 is a positive gain. The positive gain k_1 will be designed later. Equivalently, the control law (7a) can be rewritten as

$$\dot{q}_i = -k_3 \sum_{j\in\mathcal{N}_i} \omega_{ij} r_{ij} - k_1 \sum_{j\in\mathcal{N}_i^l} \left[r_{ij} - \mathrm{Mat}\left(r_{ij}^*\right) \mathrm{vec}\left(\bar{A}\right)\right].$$

For the sake of simplicity, we denote by $a \triangleq \mathrm{vec}(A)$. The updating law for the estimation $\hat{a}$ of agent 3 is given by

$$\dot{\hat{a}} = -k_2 \left(M_3^*\right)^{\mathrm{T}} M_3^* \hat{a} + k_2 \left(M_3^*\right)^{\mathrm{T}} r_3 \tag{8}$$

where $M_3^* = [\mathrm{Mat}(r_{31}^*)^{\mathrm{T}}, \mathrm{Mat}(r_{32}^*)^{\mathrm{T}}]^{\mathrm{T}} \in \mathbb{R}^{4\times 4}$, and $r_3 \triangleq [r_{31}^{\mathrm{T}}, r_{32}^{\mathrm{T}}]^{\mathrm{T}} \in \mathbb{R}^4$ for easy reading; k_2 is a positive gain to be designed.

Theorem 1: Under Assumption 1, for multiagent systems with dynamics modeled by (5), the affine formation maneuver motion governed by the linear transformation matrix A can be realized exponentially using the proposed control algorithms (7) in combination with the estimator (8), i.e., $r_{ij}(t) \to A r_{ij}^*, \forall i, j$, as $t \to \infty$. In addition, the estimation $\hat{a}$ also exponentially converges to its real value, i.e., $\hat{a}(t) \to a$, as $t \to \infty$.

Proof: Before moving on, we first define two auxiliary functions

$$f_i\left(\omega_{ij}, r_{ij}\right) \triangleq -k_3 \sum_{j\in\mathcal{N}_i} \omega_{ij} r_{ij}$$

$$g_i\left(r_{ij}, r_{ij}^*, \bar{A}\right) \triangleq -k_1 \sum_{j\in\mathcal{N}_i^l} \left(r_{ij} - \bar{A} r_{ij}^*\right).$$

TABLE I
ERROR-RELATED VARIABLES

Symbol	Quantity	Definition
$\tilde{r}_{ij}$	displacement error	$r_{ij} - Ar^*_{ij}$
$\tilde{q}_i$	absolute-like error	$q_i - Aq^*_i$
$\tilde{q}_l$	vector form	$q_l - (I_3 \otimes A)q^*_l$
$\tilde{A}$	matrix estimation error	$\hat{A} - A$
$\tilde{a}$	estimation error	$\hat{a} - a$

Throughout this article, for simplicity, we will omit the arguments when there is no ambiguity. Then, the controller (7) can be rewritten in the form of

$$\dot{q}_i = \begin{cases} f_i + g_i, & i \in \mathcal{V}_l \\ f_i, & i \in \mathcal{V}_f. \end{cases} \tag{9}$$

For clear presentation, the error-related variables are listed in Table I.

We then decompose the stability analysis of the overall closed-loop system into the following three steps:

1) the convergence of $\tilde{r}_{21}$ under $\dot{q}_i = g_i$, $i \in \mathcal{V}_l$;
2) the convergence of $\tilde{r}_{31}$, $\tilde{r}_{32}$, and $\tilde{a}$ under $\dot{q}_i = g_i$, $i \in \mathcal{V}_l$;
3) the global convergence of the desired affine formation using (9).

The first two steps aim to demonstrate the convergence of the leaders toward their desired displacements. This convergence is realized by the proposed subcontroller g_i and its associated estimator. Simultaneously, the subcontroller f_i is utilized to drive all agents to the affine image of q^*. Then, the final step is to show that the configuration q is a translation of q^*, indicating that they share the same formation shape.

For step 1), given the dynamics $\dot{q}_i = g_i$, the derivative of $\tilde{r}_{21}$ is in the form

$$\dot{\tilde{r}}_{21} = \dot{q}_2 - \dot{q}_1 = -3k_1\tilde{r}_{21}. \tag{10}$$

Therefore, we know $\tilde{r}_{21}$ converges to $\mathbf{0}_2$ exponentially fast determined by the parameter k_1, i.e., r_{12} is stabilized to r^*_{12} exponentially.

For step 2), again under the situation where the leader agents are governed by the partial input g_i, the dynamics of q_3 satisfies

$$\begin{aligned} \dot{q}_3 &= -k_1 \sum_{j\in\mathcal{N}_3^l} \left(r_{3j} - \mathrm{Mat}\left(r^*_{3j}\right)\mathrm{vec}\left(\hat{A}\right)\right) \\ &= -k_1 \sum_{j\in\mathcal{N}_3^l} \left(r_{3j} - Ar^*_{3j} + \mathrm{Mat}\left(r^*_{3j}\right)a - \mathrm{Mat}\left(r^*_{3j}\right)\hat{a}\right) \\ &= -k_1\left(\tilde{r}_{31} + \tilde{r}_{32}\right) + k_1\left(\mathbf{1}_2^{\mathrm{T}} \otimes I_2\right) M_3^*\tilde{a} \end{aligned}$$

where the third equality is obtained from Proposition 1. Then, it is easy to verify that

$$\dot{\tilde{q}}_l = -k_1\begin{bmatrix} \tilde{r}_{13} \\ \tilde{r}_{23} \\ \tilde{r}_{31} + \tilde{r}_{32} \end{bmatrix} - k_1\begin{bmatrix} \tilde{r}_{12} \\ \tilde{r}_{21} \\ 0 \end{bmatrix} + k_1\begin{bmatrix} \mathbf{0}_2 \\ \mathbf{0}_2 \\ \left(\mathbf{1}_2^{\mathrm{T}} \otimes I_2\right) M_3^*\tilde{a} \end{bmatrix} \tag{11}$$

where $\tilde{q}_l \in \mathbb{R}^6$ is the vector composed of elements $q_i - Aq^*_i$, and $q_l = [q_1^{\mathrm{T}}, q_2^{\mathrm{T}}, q_3^{\mathrm{T}}]^{\mathrm{T}}$. Now, we introduce the matrix H_s as

$$H_s \triangleq \begin{bmatrix} -1 & 0 & 1 \\ 0 & -1 & 1 \end{bmatrix}$$

whose transpose can be viewed as the incidence matrix associated with edges (3, 1) and (3, 2) and their connecting nodes. Akin to the definition of the graph Laplacian and the edge Laplacian [28], the matrices L_s and L_s^e are, respectively, defined as

$$L_s = H_s^{\mathrm{T}}H_s, \quad L_s^e = H_sH_s^{\mathrm{T}}.$$

It can be easily checked that L_s^e is positive definite. With these definitions, the compact form of (11) is written as

$$\begin{aligned} \dot{\tilde{q}}_l = &-k_1\left(L_s \otimes I_2\right)\tilde{q}_l + k_1\left([1, -1, 0]^{\mathrm{T}} \otimes I_2\right)\tilde{r}_{21} \\ &+ k_1\left(\mathrm{diag}\ (0, 0, 1) \otimes I_2\right)\left(\mathbf{1}_3\mathbf{1}_2^{\mathrm{T}} \otimes I_2\right) M_3^*\tilde{a}. \end{aligned} \tag{12}$$

In view of the updating law (8) of the parameter estimation $\hat{a}$, its error dynamics is given by

$$\begin{aligned} \dot{\tilde{a}} &= -k_2\left(M_3^*\right)^{\mathrm{T}} M_3^*\tilde{a} + k_2\left(M_3^*\right)^{\mathrm{T}}\left(r_3 - M_3^*a\right) \\ &= -k_2\left(M_3^*\right)^{\mathrm{T}} M_3^*\tilde{a} + k_2\left(M_3^*\right)^{\mathrm{T}}\tilde{r}_3 \end{aligned} \tag{13}$$

where we have inserted the term $(M_3^*)^{\mathrm{T}}M_3^*\hat{a} - (M_3^*)^{\mathrm{T}}M_3^*a$ to explicitly show up $\tilde{a}$, and the symbol $\tilde{r}_3$ is defined as $\tilde{r}_3 = [\tilde{r}_{31}^{\mathrm{T}}, \tilde{r}_{32}^{\mathrm{T}}]^{\mathrm{T}}$.

Now we consider the following sub-Lyapunov function candidate:

$$V_1 = \frac{1}{2}\tilde{r}_3^{\mathrm{T}}\left(\Xi \otimes I_2\right)\tilde{r}_3 + \frac{1}{2}\tilde{a}^{\mathrm{T}}\tilde{a}$$

where the matrix $\Xi \in \mathbb{R}^{2\times 2}$ is positive definite.

After elaborate calculation (see Appendix A), the derivative of V_1 satisfies

$$\dot{V}_1 \le -\frac{2\min\left\{\alpha, \beta\lambda_{\min}\left(\left(M_3^*\right)^{\mathrm{T}} M_3^*\right)\right\}}{\max\left\{\lambda_{\max}\left(\Xi\right), 1\right\}} V_1 + \gamma\left\|\tilde{r}_{21}\right\|^2. \tag{14}$$

Note that the coefficient of $\dot{V}_1$ on the right side is negative. Therefore, by taking account of the fact that the autonomous part of (14) is exponentially stable, it can be concluded from the input-to-state stability (ISS) theorem that V_1 converges to the origin when $\tilde{r}_{21}$ goes to zero as $t \to \infty$. Till now, the proof of step 2) is finished.

Now, we move to step 3). Consider the affine transformation $\mathcal{T}(q^*) = \{q = (I_n \otimes A)q^* + \mathbf{1}_n \otimes b | A \in \mathbb{R}^{2\times 2}, b \in \mathbb{R}^2\}$ [the matrix form of (4)], the dimension of which is 6, i.e., $\dim(\mathcal{T}(q^*)) = 6$. Assume that the basis of $\mathcal{T}(q^*)$ is denoted by $\{v_1, \ldots, v_6\}$, which are exactly the eigenvectors associated with zero eigenvalues of the matrix $(\Omega \otimes I_2)$. We define an orthogonal matrix $Q = [Q_1, Q_2]$ with $Q_1 = [v_1, \ldots, v_6]$, and the columns of $Q_2 \in \mathbb{R}^{2n\times(2n-6)}$ are eigenvectors associated with nonzero eigenvalues of $(\Omega \otimes I_2)$. Under this circumstance,

one has

$$Q^{\mathrm{T}}(\Omega \otimes I_2) Q = \begin{bmatrix} 0 & & & & \\ & \ddots & & \mathbf{0} & \\ & & 0 & & \\ & & & \lambda_7 & \\ & \mathbf{0} & & & \ddots \\ & & & & & \lambda_{2n} \end{bmatrix} \triangleq \begin{bmatrix} \Lambda_a & \\ & \Lambda_r \end{bmatrix} \tag{15}$$

where $\Lambda_a \in \mathbb{R}^{6\times 6}$, and $\Lambda_r \in \mathbb{R}^{(2n-6)\times(2n-6)}$.

Consider the system dynamics $\dot{q}_i = f_i$, i.e.,

$$\dot{q}_i = -k_3 \sum_{j\in\mathcal{N}_i} \omega_{ij}\left(q_i - q_j\right).$$

The compact form is written as

$$\dot{q} = -k_3 (\Omega \otimes I_2) q.$$

To analyze the stability and its equilibria, we conduct the coordinate transformation as

$$p = \begin{bmatrix} p_a \\ p_r \end{bmatrix} = Q^{\mathrm{T}} q.$$

The dynamics of p is given by

$$\dot{p} = Q^{\mathrm{T}}\dot{q} = -k_3 Q^{\mathrm{T}}(\Omega \otimes I_2) Q p.$$

In view of (15), one has

$$\begin{cases} \dot{p}_a = \mathbf{0} \\ \dot{p}_r = -k_3 \Lambda_r p_r. \end{cases}$$

From the positive definiteness of the matrix Λ_r, we know p_r exponentially converges to zero. This implies $Q_2^{\mathrm{T}} q \to \mathbf{0}$, as $t \to \infty$. Note that $Q_2^{\mathrm{T}} Q_1 = \mathbf{0}$, then this means q converges to the subspace spanned by the matrix Q_1, which is exactly the affine transformation of q^*. Therefore, we conclude that q converges to $\mathcal{T}(q^*)$ exponentially fast.

Now we consider the overall dynamics (9). Based on the previous analyses and the linear property of the two dynamics $\dot{q} = f(q)$ and $\dot{q} = g(q)$, from the results in [7, Theorem 7.2] and [29], we arrive at the conclusion that all the agents converge to the desired formation determined by the matrix A, i.e., $r_{ij}(t) \to A r_{ij}^*$, $\forall i, j$, as $t \to \infty$. In addition, from the exponential convergence property, we also know that the formation parameters can be precisely estimated, i.e., $\hat{a}(t) \to a$, as $t \to \infty$. □

IV. Affine Formation Maneuver Control Under Time-Varying Matrix $A(t)$

In this section, we consider the situation where the desired formation is dynamically governed by the time-varying linear transformation matrix $A(t)$.

Without loss of generality, it is assumed that the signal $\mathrm{vec}(A(t))$ [i.e., $a(t)$] is generated by the following exosystem:

$$\dot{v}(t) = S v(t) \tag{16a}$$

$$a(t) = C v(t) \tag{16b}$$

where $v(t) \in \mathbb{R}^p$, $S \in \mathbb{R}^{p\times p}$, and $C \in \mathbb{R}^{4\times p}$ are the constant matrices, and the system (16a) is marginally stable. We will omit the argument t when it is clear that we are referring to $a(t)$, $v(t)$, and $A(t)$.

The focus of [8], [9], and [10] is to design control algorithms only for followers to track the stabilized leaders. However, in this article, we consider an integrated control framework not only for followers but also for leaders. Partially motivated by Zhao [8], where the strategy for tracking the dynamic leader is discussed, the kernel of this section is to investigate the control strategy for leaders, part of whom has no access to the prescribed formation parameter. Hence, the main challenge lies in controlling the unaware leader while inferring the unknown parameter from the low-order relative displacements with regard to the dynamic reference signals. The control law to deal with the time-varying formation parameter has the same merit as that in Section III, namely, the leaders are responsible for managing the geometric formation shape and the followers move in consistent with the inner coupling strength ω_{ij}.

The control laws for each agent are designed as

$$u_i = -k_1 \sum_{j\in\mathcal{N}_i^l} \left(r_{ij} - \bar{A} r_{ij}^*\right) + \frac{1}{3}\dot{\bar{A}} \sum_{j\in\mathcal{N}_i^l} r_{ij}^*, \quad i \in \mathcal{V}_l \tag{17a}$$

$$u_i = -\frac{1}{d_i} \sum_{j\in\mathcal{N}_i} \omega_{ij}\left[\left(q_i - q_j\right) - \dot{q}_j\right], \quad i \in \mathcal{V}_f \tag{17b}$$

where k_1 is a positive gain. $d_i = \sum_{j\in\mathcal{N}_i} \omega_{ij}$ is a nonzero constant. $\bar{A}$ follows the same definition in (7), and $\dot{\bar{A}}$ denotes its derivative, i.e.,

$$\dot{\bar{A}} = \begin{cases} \dot{A}, & i = 1, 2 \\ \dot{\hat{A}}, & i = 3 \end{cases}$$

with $\dot{\hat{A}}$ derived from $\dot{\hat{v}}$ and $\hat{a}$, given by

$$\begin{cases} \dot{z} = Fz + D \sum\limits_{j\in\mathcal{N}_3^l} \left(q_3 - q_j\right) \\ \hat{v} = T^{-1} z \\ \hat{a} = C\hat{v} \end{cases} \tag{18}$$

where $F \in \mathbb{R}^{p\times p}$ is chosen to be Hurwitz, $T \in \mathbb{R}^{p\times p}$ is nonsingular, and $D \in \mathbb{R}^{p\times 2}$ will be defined later. Note that the implementation of (18) only depends on the local information, i.e., $q_3 - q_j$, $j = 1, 2$. Following the analysis in Section III, the displacement r_{21} converges to its real value without any bias, i.e., $\tilde{r}_{21} \to \mathbf{0}$, since agents 1 and 2 have the full knowledge of A and its derivative.

Regarding the time-varying linear transformation matrix parameter, we have the following main result, giving an integrated control framework to realize more flexible affine formation maneuver control with full DOF in shape morphing.

Theorem 2: Consider a group of multiagent systems modeled by (5), whose formation shape is determined by the time-varying linear transformation matrix $A(t)$ (or its equivalent vector form) generated via (16). Under Assumption 1,

by employing the control algorithm given in (17) together with the estimation law (18), the agents can be stabilized at the specified formation, i.e., $r_{ij}(t) \to A(t)r_{ij}^*, \forall i, j$, as $t \to \infty$, if there exists a solution for T to the following Sylvester equation:

$$FT - TS + \Phi = 0 \tag{19}$$

where $\Phi = D(\mathbf{1}_2^{\mathrm{T}} \otimes I_2)M_3^*C$, and $3F + 2\Phi T^{-1}$ is Hurwitz. Simultaneously, the precise estimation of the time-varying formation maneuver parameter can also be obtained, i.e., $\hat{v}(t) \to v(t)$ [equivalently, $\hat{a}(t) \to a(t)$], as $t \to \infty$.

Proof: It has been recognized in [8] that the control law (17b) for followers can render zero steady-state tracking error, i.e., $\sum_{j\in\mathcal{N}_i} \omega_{ij}(q_i - q_j) \to 0$, as $t \to \infty$. Under this circumstance, we know the entire formation will converge to its predefined shape determined by the affine transformation parameters once the leaders reach their target relative displacements. Hence, with this "cascade structure," we concentrate on the convergence analysis of displacement errors $\tilde{r}_{31}$ and $\tilde{r}_{32}$. Recalling the definition that $M_3^* = [\mathrm{Mat}(r_{31}^*)^{\mathrm{T}}, \mathrm{Mat}(r_{32}^*)^{\mathrm{T}}]^{\mathrm{T}}$ and applying the operation of adding and subtracting the same term $D\sum_{j\in\mathcal{N}_3^l} A(q_3^* - q_j^*)$ into the first line of (18), one has

$$\begin{cases} \dot{z} = Fz + D\left(\mathbf{1}_2^{\mathrm{T}} \otimes I_2\right)\left(M_3^*Cv + \tilde{r}_3\right) \\ \hat{v} = T^{-1}z \\ \hat{a} = C\hat{v}. \end{cases} \tag{20}$$

For the formation parameter estimation, we introduce an auxiliary variable

$$e = z - Tv.$$

Then, it is straightforward to know $e = T\tilde{v} \triangleq T(\hat{v} - v)$. For the sake of brief presentation, let $E \triangleq \mathbf{1}_2^{\mathrm{T}} \otimes I_2$, $\Psi \triangleq EM_3^*C$, and thus, $\Phi = D\Psi$. Thus, in combination with the dynamics (16) and (20), the dynamics of e is given by

$$\dot{e} = Fe + (FT - TS + \Phi)v + DE\tilde{r}_3.$$

From Theorem 2, under the condition that the Sylvester equation (19) has solutions, $\dot{e}$ can be stated as

$$\dot{e} = Fe + DE\tilde{r}_3. \tag{21}$$

Giving consideration of the control system $\dot{q}_i = g_i$ in (17), there holds

$$\dot{\tilde{r}}_{31} = -3k_1\tilde{r}_{31} + k_1\Psi T^{-1}e + \frac{1}{3}\Psi T^{-1}\left(Fe + DE\tilde{r}_3\right).$$

The detailed calculation process is given in Appendix B. Akin to the expression of $\dot{\tilde{r}}_{31}$, we can obtain the corresponding form of $\dot{\tilde{r}}_{32}$. Recalling the equality that $E\tilde{r}_3 = \tilde{r}_{31} + \tilde{r}_{32}$. For the sake of brevity in notation, we define $\eta \triangleq E\tilde{r}_3 \in \mathbb{R}^{2\times 1}$, whose dynamics is formulated as

$$\dot{\eta} = -3k_1\eta + 2k_1\Psi T^{-1}e + \frac{2}{3}\Psi T^{-1}\left(Fe + D\eta\right). \tag{22}$$

It can be observed in (22) that the formula within the parentheses on the right side is exactly $\dot{e}$. By virtue of such a coupling relationship and aiming to derive a concise expression in terms of the errors η and e, we introduce a new variable

$$\xi \triangleq \eta - \frac{2}{3}\Psi T^{-1}e.$$

Taking the derivative of ξ and substituting (21) and (22) yields

$$\dot{\xi} = \dot{\eta} - \frac{2}{3}\Psi T^{-1}\dot{e} = -3k_1\xi. \tag{23}$$

It is straightforward to know $\xi \to 0$ exponentially, which equivalently implies $\eta \to (2/3)\Psi T^{-1}e$. With this convergence property, (21) can be rewritten as

$$\dot{e} = \frac{1}{3}\left(3F + 2D\Psi T^{-1}\right)e. \tag{24}$$

Hence, one concludes from the Hurwitz stability of matrix $3F + 2\Phi T^{-1}$ that e decays to 0 at exponential speed, i.e., the formation maneuver parameter $\hat{v}$ converges to its real value v exponentially. In view of the estimator (18), the components of matrix $A(t)$ can be precisely derived, namely, $\hat{a}(t) \to a(t)$, as $t \to \infty$, which in turn implies $E\tilde{r}_3 \to 0$ from (21). Following the same line of Section III, we know $\lim_{t\to\infty} r_{3i}(t) - A(t)r_{3i}^* = 0, i = 1, 2$. This completes the proof. □

Remark 3: The condition for the existence of the solution to Sylvester equations can be found in [30] and [31], where specific numerical algorithms for solving Sylvester equations are also presented, such as the Hessenberg–Schur method.

V. Simulation and Experimental Results

In this section, we validate the theoretical results of the proposed estimation-based affine formation maneuver control frameworks through numerical simulations and experiments.

A. Numerical Simulations

The simulation is conducted to validate the presented results from Theorems 1 and 2. Hence, two cases are, respectively, considered: constant and time-varying linear transformation matrix A. In both cases, the formation team consists of 100 agents, whose nominal configuration is generated by

$$q_i^* = \begin{bmatrix} \left(r + \frac{Ri}{100}\right)\cos\left(\frac{1}{2}\pi\sqrt{i}\right) \\ \left(r + \frac{Ri}{100}\right)\sin\left(\frac{1}{2}\pi\sqrt{i}\right) \end{bmatrix}, \quad i = 1, \ldots, 100.$$

where $r = 3$ and $R = 20$ are selected.

Their interaction relationship is shown in Fig. 2, whose associated stress matrix[1] is computed by the topological optimization given in [26] (similar to [32] and [33], alternating direction method of multipliers (ADMM) [34] is applied to accelerate the solving process). We designate agents 49, 75, and 99 as the leaders that control the variation of the entire formation, namely, $\mathcal{V}_l = \{49, 75, 99\}$.

[1] https://github.com/mkb9559/stress-matrix-100

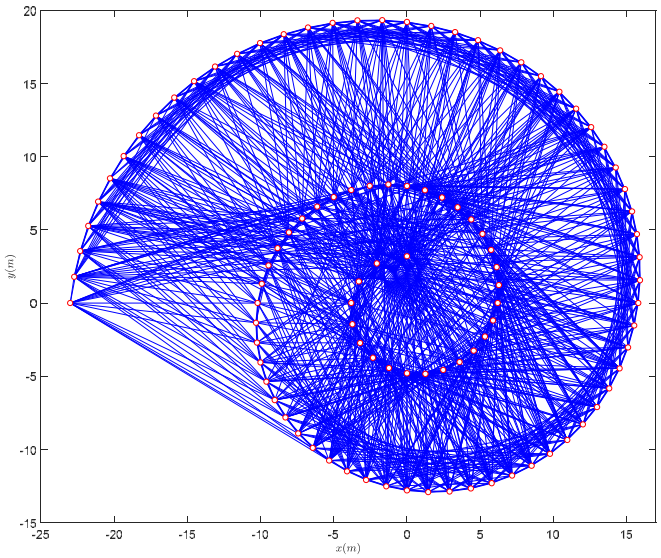

Fig. 2. Nominal formation with 100 agents.

1) Formation Control Under Constant A: To show the effectiveness of the proposed estimation-based control (7) and (8), we set the transformation $\mathrm{vec}(A) = a$ as

$$a = \begin{cases} \begin{bmatrix} 3 & 0 & 0 & 3 \end{bmatrix}^{\mathrm{T}}, & 0 \text{ s} \le t < 70 \text{ s} \\ \begin{bmatrix} 2.2 & 0 & 0 & 1.2 \end{bmatrix}^{\mathrm{T}}, & 70 \text{ s} \le t < 300 \text{ s} \\ \begin{bmatrix} 3 & 0 & 0 & 3 \end{bmatrix}^{\mathrm{T}}, & 300 \text{ s} \le t \end{cases} \tag{25}$$

which is actually a piecewise function of t, a slight extension to the constant matrix A. The corresponding control parameters are set as $k_1 = 11$, $k_2 = 1.6$, and $k_3 = 1$. The initial position of agents are randomly generated around the origin. A feedforward velocity along the x+-direction is added to all agents' formation controllers for a maneuver task.

The simulation results are presented in Figs. 3–5. Formation variations during the simulation are illustrated in Fig. 3. At $t = 34$ s, it sees that formation stabilization is achieved from the random initialization. Then, the team of agents shrinks their formation and passes through a narrow area with obstacles. After that, agents recover to stretched formation at $t = 323$ s. For the linked agents, the convergence to the prescribed distances is shown in Fig. 4, which means the desired formation maneuver is achieved. From Fig. 5, it is clearly seen that the precise estimation can be obtained using our proposed algorithm (8), providing guidance for other agents in the integrated estimation-control framework.

2) Formation Control Under Time-Varying $A(t)$: Without loss of generality, it is assumed that the matrices S and C of the exosystem (16) are

$$S = \begin{bmatrix} 0 & -0.2 & 0 & 0 \\ 0.1 & 0 & 0 & 0 \\ 0 & 0.4 & 0 & 0.14 \\ 0 & 0 & -0.2 & 0 \end{bmatrix}$$

$$C = \begin{bmatrix} 0.8 & 0 & 0 & 0.8 \\ 0 & 0 & 0.4 & 0 \\ 0 & -0.56 & 0.56 & 0 \\ 0.8 & 0 & 0 & 0.8 \end{bmatrix}.$$

Under the constraints imposed on matrices F, D, and T in Theorem 2, we choose

$$F = \begin{bmatrix} -1 & 0 & 0.2 & 0 \\ 0 & -1 & 0 & 0 \\ 0 & 2 & -1 & 0 \\ 2 & 0 & 0 & -1 \end{bmatrix}, \quad D = \begin{bmatrix} 1 & 0 \\ 0 & 1 \\ 1 & 0 \\ 0 & 1 \end{bmatrix}$$

$$T = \begin{bmatrix} 0.2219 & 1.1102 & 1.2965 & 0.1126 \\ -1.5683 & -0.3168 & 0.0778 & -1.6109 \\ -2.3355 & -0.0114 & 0.7697 & -2.5296 \\ -1.3409 & 1.8465 & 2.6439 & -1.7450 \end{bmatrix}.$$

It can be verified that these choices satisfy the requirements of the Hurwitz condition and the Sylvester equation (19) with respect to certain specific matrices. Then, we implement the controller (17) and the corresponding estimator (18) with $k_1 = 1$. The simulation results are presented in Figs. 6 and 7. The distance of linked agents convergent to the prescribed time-varying distances, as shown in Fig. 6. It is also clearly shown in Fig. 7 that the precise estimation is obtained, which supports the achievement of the desired time-varying formation maneuver.

B. Experiments

In this section, we test the performances of our proposed theoretical results on a group of Crazyflie 2.0[2] flying robots, as shown in Fig. 8. The framework of the experiment system is presented in Fig. 9. The positioning information of each robot is provided by the auxiliary OptiTrack[3] motion capture system through recording the movements of the markers placed on the top of robots (Fig. 8).

Crazyfile supports a variety of control modes [35], [36]. The API "cmdVelocityWorld()" [37] supports velocities as control inputs, which is exactly suitable for the considered integrator systems (5) in this study. In this situation, the inputs are actually the velocity commands, and thus, the positions can be directly regulated. The flying robots communicate with the ground control station (a PC) via Crazyradio PA[4] data transmission module.

It is considered four Crazyflies in experiments. Agents 1–3 are selected as the leaders that control the variation of the entire formation, namely, $\mathcal{V}_l = \{1, 2, 3\}$. The square nominal formation and associated stress matrix are given as follows:

$$q_1^* = \begin{bmatrix} -0.5 & 0.5 \end{bmatrix}^{\mathrm{T}}$$
$$q_2^* = \begin{bmatrix} 0.5 & 0.5 \end{bmatrix}^{\mathrm{T}}$$
$$q_3^* = \begin{bmatrix} 0.5 & -0.5 \end{bmatrix}^{\mathrm{T}}$$
$$q_4^* = \begin{bmatrix} -0.5 & -0.5 \end{bmatrix}^{\mathrm{T}} \quad \Omega = \begin{bmatrix} -1 & 1 & -1 & 1 \\ 1 & -1 & 1 & -1 \\ -1 & 1 & -1 & 1 \\ 1 & -1 & 1 & -1 \end{bmatrix}.$$

[2]https://www.bitcraze.io/products/crazyflie-2-1/
[3]https://www.optitrack.com/
[4]https://www.bitcraze.io/products/crazyradio-pa/

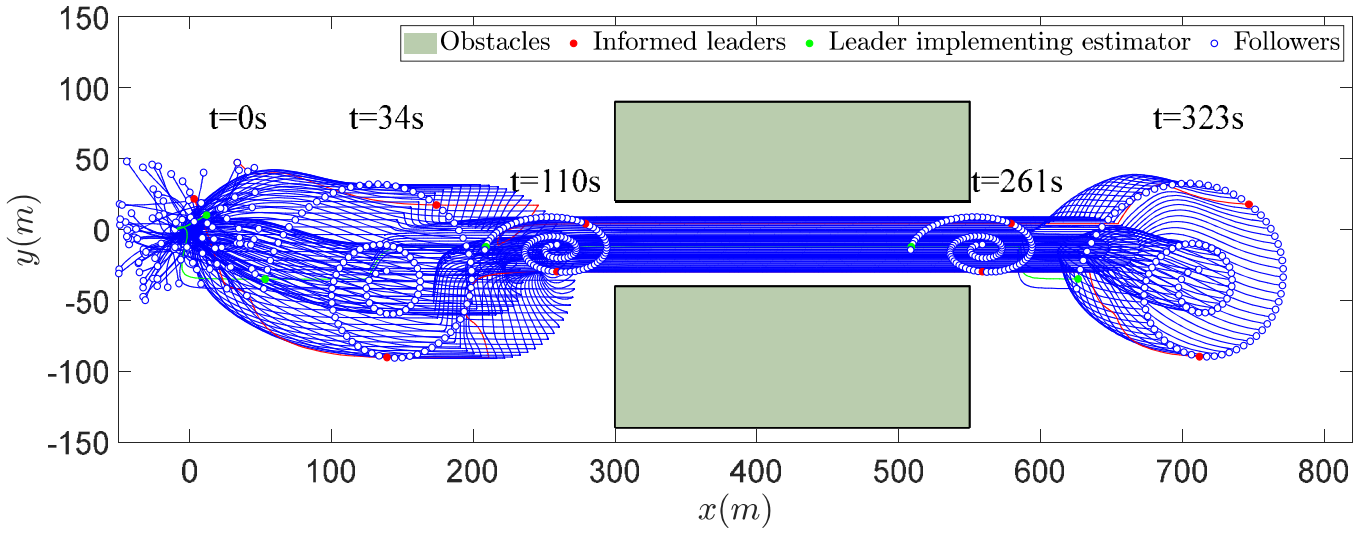

Fig. 3. Formation variations with constant A in simulation.

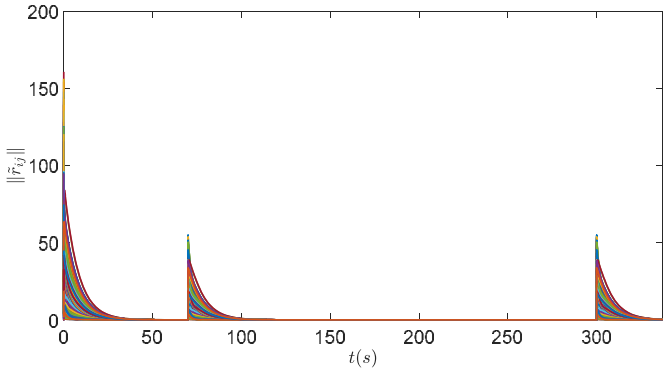

Fig. 4. Distance convergence errors of pairwise agents using the proposed control law (7) and associated estimator (8). It is shown that the distance convergence errors are stabilized at the origin in different phases, which are consistent with the change of A defined in (25).

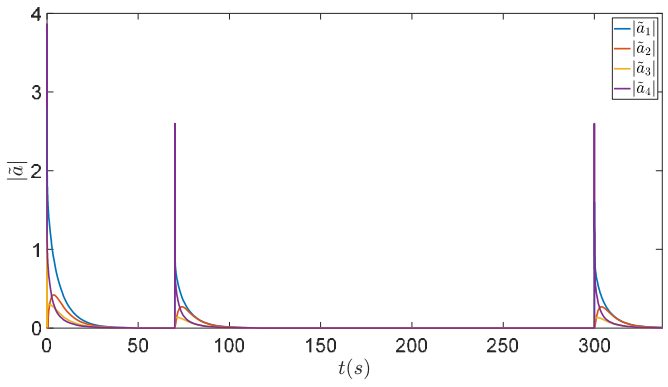

Fig. 5. Componentwise estimation errors with respect to the linear transformation matrix A. All the errors converge to zero in accordance with the variation of A, implying the precise identification via the proposed estimator (8).

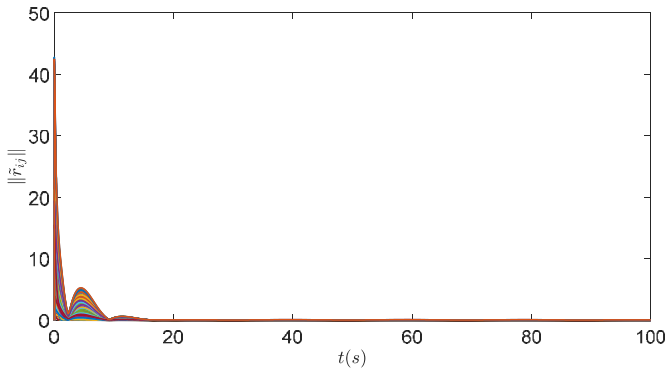

Fig. 6. Distance convergence errors of pairwise agents using the proposed control law (17) and associated estimator (18). It is shown that the distance convergence errors are stabilized at the origin, which also means that the exosystem-generated time-varying A is well-estimated.

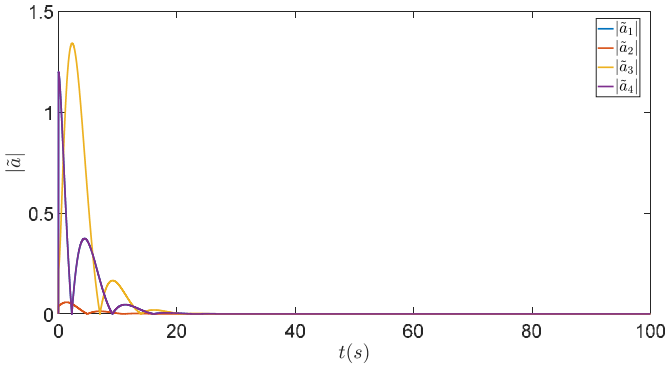

Fig. 7. Componentwise estimation errors with respect to the time-varying linear transformation matrix A. All the errors converge to zero, implying the precise identification via the proposed estimator (18).

1) Experiment Under Constant Matrix A: Considering the limited flight time of the Crazyflie and the constrained experimental space, we set the appropriate formation transformation parameter $\mathrm{vec}(A) = a$ as

$$a = \begin{cases} \begin{bmatrix} 1 & 0 & 0 & 1 \end{bmatrix}^{\mathrm{T}}, & 0\ \mathrm{s} \le t < 21.5\ \mathrm{s} \\ \begin{bmatrix} -1 & 0.5 & 0.8 & 1 \end{bmatrix}^{\mathrm{T}}, & t \ge 21.5\ \mathrm{s} \end{cases} \tag{26}$$

Fig. 8. Crazyflie flying robot with OptiTrack marker.

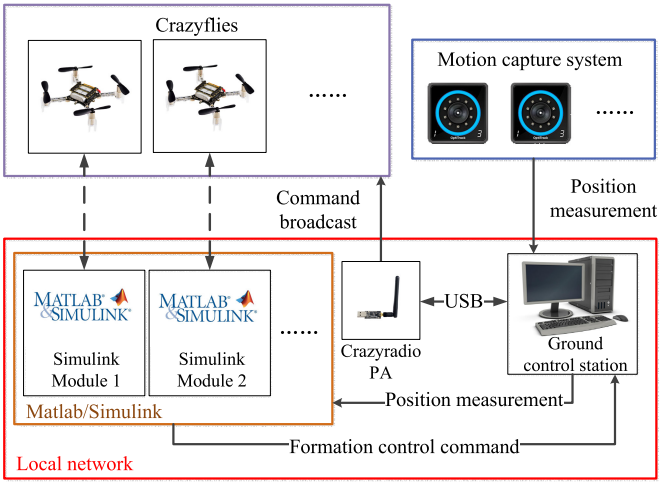

Fig. 9. Structure and information flow of the experimental system. The designed controllers and estimators are deployed on Simulink modules. We use "robotlib/Subscribe" and "robotlib/Publish" blocks to communicate with the ground control station PC, which runs an ROS master for data transferring between MATLAB and Crazyflie.

which is a piecewise constant function of t. The initial positions are given by

$$q_1(0) = \begin{bmatrix}-1 & 0.5\end{bmatrix}^{\mathrm{T}} \quad q_2(0) = \begin{bmatrix}1 & 0.5\end{bmatrix}^{\mathrm{T}}$$
$$q_3(0) = \begin{bmatrix}1 & -0.5\end{bmatrix}^{\mathrm{T}} \quad q_4(0) = \begin{bmatrix}-1 & 0.5\end{bmatrix}^{\mathrm{T}}.$$

The corresponding parameters are set as $k_1 = 11$, $k_2 = 1.6$, and $k_3 = 1$ in the implementation of (7) and (8), under which the snapshots illustrating formation transformation process can be found in Fig. 10. The consistency between the desired formation parameter and the observed formation change is readily apparent. This is further verified by the distance convergence errors depicted in Fig. 11. Regarding the estimation performance, Fig. 12 presents the estimation errors for each component with respect to the linear transformation matrix A, affirming the effectiveness of the proposed estimation-based method.

2) Experiment Under Time-Varying Matrix A: In this scenario, the initial configuration of Crazyflies is identical to that in Section V-B1. The exosystem generating the time-varying A, as well as the associated matrix parameters F, D, and T, remains consistent with the setup detailed in Section V-A2. By implementing the proposed controller (17) and the corresponding estimator (18) with $k_1 = 1$, the experimental results are presented in Figs. 13–15. The snapshots capturing the

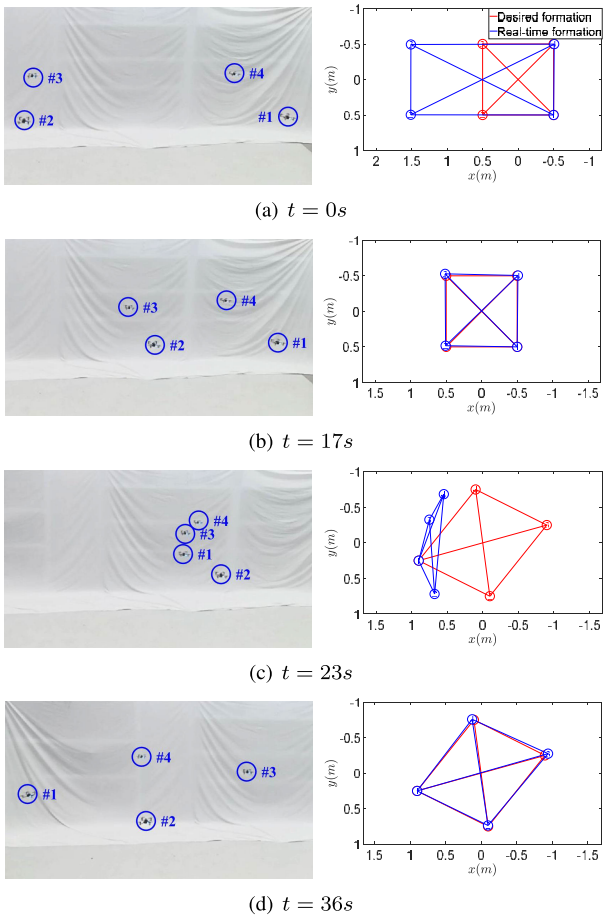

Fig. 10. Experimental results of formation flying conducted on four Crazyflie robots utilizing our proposed control scheme outlined in (7) and (8). The left column shows the spatial distribution of robots at various time instants, while the corresponding Cartesian coordinates are displayed in the right column, marked in blue. The desired formation configuration is highlighted in red. (a) and (b) Progressive formation change associated with vec(A) during the first phase. (c) At $t = 17$ s, it is evident that the robots have achieved the desired formation. Subsequently, as the formation parameter changes from 21.5 s, the entire formation undergoes a transformation to the new configuration. (d) Finally, at $t = 36$ s, the formation successfully converges to its newly prescribed pattern.

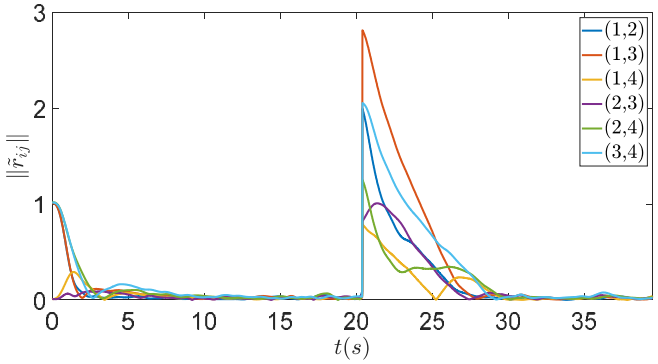

Fig. 11. Distance convergence errors of pairwise robots using the proposed control law (7) and the associated estimator (8). The results demonstrate that the distance convergence errors consistently stabilize at the origin following each change of the parameter A as defined in (26).

evolution of the formation during the transformation process are presented in Fig. 13. The Crazyflie robots are stabilized

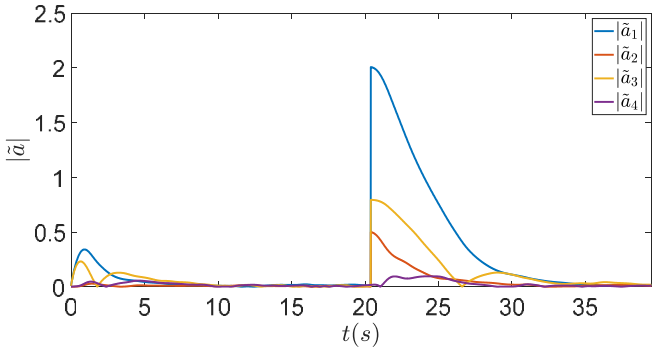

Fig. 12. Componentwise estimation errors with respect to the linear transformation matrix A. It is observed that all errors consistently converged to zero, aligning with the variations in A. These findings indicate the accurate identification achieved through the proposed estimator (8).

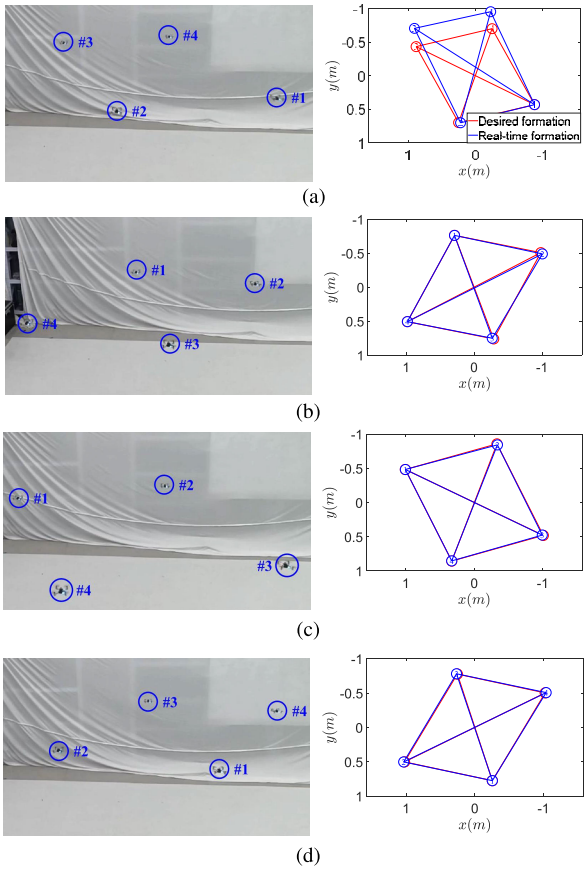

Fig. 13. Experimental results using the proposed estimation-control scheme (17) and (18). Upon reviewing all the snapshots and comparing them with the desired formation shape, it is evident that the team Crazyflie robots move in an organized pattern, regardless of the variations in geometric shapes. This adaption to different shapes is consistent with the time-varying linear transformation matrix $A(t)$. (a) $t = 5$ s. (b) $t = 15$ s. (c) $t = 25$ s. (d) $t = 35$ s.

at the desired relative distances with respect to its neighbors are shown in Fig. 14, indicating convergence toward the desired formation. Correspondingly, Fig. 15 reveals that the precise knowledge of $A(t)$ is accurately inferred through the application of the strategy (18).

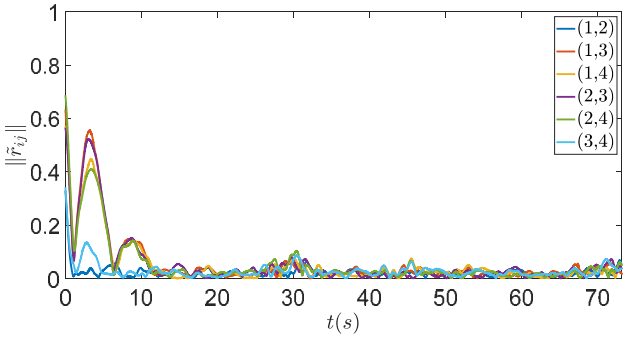

Fig. 14. Distance convergence errors between pairwise robots in the experiment. It is observed that the errors quickly stabilized at the origin after a brief period of adjustments.

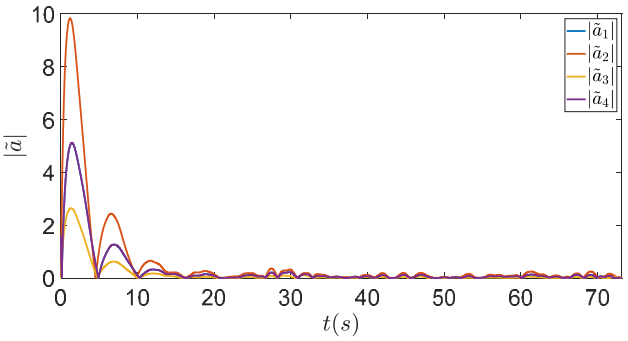

Fig. 15. Componentwise estimation errors with respect to $A(t)$. The observed convergence clearly demonstrates the effectiveness of estimating time-varying parameters using limited measurements.

VI. Conclusion

This article presents a comprehensive exploration of the planar affine formation maneuver control strategy, wherein the variation in formation shape is characterized by a matrix parameter. With partially informed leaders, we have proposed a joint estimation and control scheme for multiagent systems that leverages local displacements. Through this scheme, the unaware leader can accurately infer the unknown matrix parameter. Specifically, only two leaders need to possess the knowledge of the target linear transformation matrix A, while the remaining leaders can estimate A based on their locally measured relative displacements. Such an intrinsically interactive structure makes the proposed technique find applicability in cooperative surveillance or monitoring tasks with limited communication, and requiring information security. We develop two distinct strategies, incorporating distributed controllers and associated estimators, to handle scenarios involving both constant and time-varying formation parameters $A(t)$. The presented simulations also verified the effectiveness of large-scale formation tasks. Future research directions involve exploring estimation techniques with less available information and handling arbitrary, more complex time-varying matrices $A(t)$.

Appendix A
Calculation of $\dot{V}_1$

Noting that $\tilde{r}_3 = (H_s \otimes I_2)\tilde{q}_l$, the derivative of V_1 satisfies

$$\dot{V}_1 = \frac{1}{2}\dot{\tilde{r}}_3^{\mathrm{T}}(\Xi \otimes I_2)\tilde{r}_3 + \frac{1}{2}\tilde{r}_3^{\mathrm{T}}(\Xi \otimes I_2)\dot{\tilde{r}}_3 + \tilde{a}^{\mathrm{T}}\dot{\tilde{a}}$$

$$= \tilde{r}_3^{\mathrm{T}} (\Xi \otimes I_2) \dot{\tilde{r}}_3 + \tilde{a}^{\mathrm{T}} \dot{\tilde{a}}$$
$$= \left[(H_s \otimes I_2)\tilde{q}_l\right]^{\mathrm{T}} (\Xi \otimes I_2)(H_s \otimes I_2)\dot{\tilde{q}}_l + \tilde{a}^{\mathrm{T}}\dot{\tilde{a}} \quad (27)$$

where the last equality is derived by invoking the symmetry property of Ξ. Replacing $\dot{\tilde{q}}_l$ and $\dot{\tilde{a}}$ in the last equation by (12) and (13), respectively, we have

$$\begin{aligned}
\dot{V}_1 = {} & \left[(H_s \otimes I_2)\tilde{q}_l\right]^{\mathrm{T}} (\Xi \otimes I_2)(H_s \otimes I_2) \\
& \times \left(-k_1 \left(H_s^{\mathrm{T}} H_s \otimes I_2\right)\tilde{q}_l \right. \\
& \quad + k_1 \left([1,-1,0]^{\mathrm{T}} \otimes I_2\right)\tilde{r}_{21} \\
& \quad \left. + k_1 \left(\mathrm{diag}\ (0,0,1) \otimes I_2\right)\left(\mathbf{1}_3\mathbf{1}_2^{\mathrm{T}} \otimes I_2\right) M_3^* \tilde{a}\right) \\
& + \tilde{a}^{\mathrm{T}} \left(-k_2 \left(M_3^*\right)^{\mathrm{T}} M_3^* \tilde{a} + k_2 \left(M_3^*\right)^{\mathrm{T}} \tilde{r}_3\right) \\
= {} & -k_1 \left[(H_s \otimes I_2)\tilde{q}_l\right]^{\mathrm{T}} (\Xi \otimes I_2)\left(H_s H_s^{\mathrm{T}} \otimes I_2\right)(H_s \otimes I_2)\tilde{q}_l \\
& + k_1 \left[(H_s \otimes I_2)\tilde{q}_l\right]^{\mathrm{T}} (\Xi \otimes I_2)\left([-1,1]^{\mathrm{T}} \otimes I_2\right)\tilde{r}_{21} \\
& + k_1 \left[(H_s \otimes I_2)\tilde{q}_l\right]^{\mathrm{T}} (\Xi \otimes I_2)\left(\begin{bmatrix} 1 & 1 \\ 1 & 1 \end{bmatrix} \otimes I_2\right) M_3^* \tilde{a} \\
& - k_2 \left(M_3^* \tilde{a}\right)^{\mathrm{T}} M_3^* \tilde{a} + k_2 \left(M_3^* \tilde{a}\right)^{\mathrm{T}} \tilde{r}_3. \quad (28)
\end{aligned}$$

By employing Young's inequality for real numbers, we obtain that

$$\begin{aligned}
\dot{V}_1 \le {} & -k_1 \lambda_{\min}\left(\Xi L_s^e\right)\|\tilde{r}_3\|^2 + k_1 \lambda_{\max}\left(\Xi \mathbf{1}_2 \mathbf{1}_2^{\mathrm{T}}\right)\|\tilde{r}_3\|\left\|M_3^*\tilde{a}\right\| \\
& - k_2 \left\|M_3^*\tilde{a}\right\|^2 + k_2 \left\|M_3^*\tilde{a}\right\|\|\tilde{r}_3\| \\
& + \sqrt{2} k_1 \lambda_{\max}(\Xi)\|\tilde{r}_3\|\|\tilde{r}_{21}\| \\
\le {} & -k_1 \lambda_{\min}\left(\Xi L_s^e\right)\|\tilde{r}_3\|^2 - k_2 \left\|M_3^*\tilde{a}\right\|^2 \\
& + \frac{k_1}{2}\lambda_{\max}\left(\Xi \mathbf{1}_2 \mathbf{1}_2^{\mathrm{T}}\right)\|\tilde{r}_3\|^2 + \frac{k_1}{2}\lambda_{\max}\left(\Xi \mathbf{1}_2 \mathbf{1}_2^{\mathrm{T}}\right)\left\|M_3^*\tilde{a}\right\|^2 \\
& + \frac{k_2}{2}\|\tilde{r}_3\|^2 + \frac{k_2}{2}\left\|M_3^*\tilde{a}\right\|^2 \\
& + \sqrt{2} k_1 \lambda_{\max}(\Xi)\left(\frac{\epsilon}{2}\|\tilde{r}_3\|^2 + \frac{1}{2\epsilon}\|\tilde{r}_{21}\|^2\right) \\
\le {} & -\left(k_1 \lambda_{\min}\left(\Xi L_s^e\right) - \frac{k_1}{2}\lambda_{\max}\left(\Xi \mathbf{1}_2 \mathbf{1}_2^{\mathrm{T}}\right) - \frac{k_2}{2}\right. \\
& \left. - \frac{\epsilon\sqrt{2} k_1}{2}\lambda_{\max}(\Xi)\right)\|\tilde{r}_3\|^2 \\
& - \left(k_2 - \frac{k_1}{2}\lambda_{\max}\left(\Xi \mathbf{1}_2 \mathbf{1}_2^{\mathrm{T}}\right) - \frac{k_2}{2}\right)\left\|M_3^*\tilde{a}\right\|^2 \\
& + \frac{\sqrt{2} k_1}{2\epsilon}\lambda_{\max}(\Xi)\|\tilde{r}_{21}\|^2 \\
\triangleq {} & -\alpha\|\tilde{r}_3\|^2 - \beta\left\|M_3^*\tilde{a}\right\|^2 + \gamma\|\tilde{r}_{21}\|^2 \quad (29)
\end{aligned}$$

where ϵ is chosen to be a small positive number, such that

$$\begin{cases} \lambda_{\min}\left(\Xi L_s^e\right) > \lambda_{\max}\left(\Xi \mathbf{1}_2 \mathbf{1}_2^{\mathrm{T}}\right) + \epsilon\sqrt{2}/2\lambda_{\max}(\Xi) \\ k_2 > k_1 \lambda_{\max}\left(\Xi \mathbf{1}_2 \mathbf{1}_2^{\mathrm{T}}\right). \end{cases} \quad (30)$$

It can be proven that if the matrix Ξ and the small number ϵ are chosen satisfying (30), then the coefficients α and β will always be positive. In this context, when ϵ is sufficiently small, one available choice of Ξ satisfying (30) is

$$\begin{bmatrix} 1 & -0.5 \\ -0.5 & 1 \end{bmatrix}.$$

Under the given condition that the leaders linearly span $\mathbb{R}^2$, we know that the matrix M_3^* is full rank. Notice that

$$\|M_3^*\tilde{a}\|^2 = \tilde{a}^{\mathrm{T}}\left(M_3^*\right)^{\mathrm{T}} M_3^* \tilde{a} \ge \lambda_{\min}\left(\left(M_3^*\right)^{\mathrm{T}} M_3^*\right)\|\tilde{a}\|^2.$$

Hence, $\dot{V}_1$ in (29) satisfies

$$\begin{aligned}
\dot{V}_1 & \le -\alpha\|\tilde{r}_3\|^2 - \beta\lambda_{\min}\left(\left(M_3^*\right)^{\mathrm{T}} M_3^*\right)\|\tilde{a}\|^2 + \gamma\|\tilde{r}_{21}\|^2 \\
& \le -\min\left\{\alpha, \beta\lambda_{\min}\left(\left(M_3^*\right)^{\mathrm{T}} M_3^*\right)\right\}\left(\|\tilde{r}_3\|^2 + \|\tilde{a}\|^2\right) \\
& \quad + \gamma\|\tilde{r}_{21}\|^2. \quad (31)
\end{aligned}$$

Recalling that for the sub-Lyapunov function V_1, there holds

$$\begin{aligned}
V_1 &= \frac{1}{2}\tilde{r}_3^{\mathrm{T}}(\Xi \otimes I_2)\tilde{r}_3 + \frac{1}{2}\tilde{a}^{\mathrm{T}}\tilde{a} \\
&\le \frac{1}{2}\max\{\lambda_{\max}(\Xi), 1\}\left(\|\tilde{r}_3\|^2 + \|\tilde{a}\|^2\right).
\end{aligned}$$

Then, (31) can be rewritten as

$$\dot{V}_1 \le -\frac{2\min\left\{\alpha, \beta\lambda_{\min}\left(\left(M_3^*\right)^{\mathrm{T}} M_3^*\right)\right\}}{\max\{\lambda_{\max}(\Xi), 1\}} V_1 + \gamma\|\tilde{r}_{21}\|^2.$$

Appendix B
Calculation of $\dot{r}_{31}$

Under the assumption that $\dot{q}_i = g_i$ with g_i given in (17), one has

$$\begin{aligned}
\dot{\tilde{r}}_{31} = {} & -k_1\left(r_{31} - \hat{A}r_{31}^* + r_{32} - \hat{A}r_{32}^*\right) \\
& + k_1\left(r_{12} - Ar_{12}^* + r_{13} - Ar_{13}^*\right) \\
& + \frac{1}{3}\left(\dot{\hat{A}}r_{31}^* + \dot{\hat{A}}r_{32}^*\right) - \frac{1}{3}\left(\dot{A}r_{12}^* + \dot{A}r_{13}^*\right) \\
& - \dot{A}r_{31}^*.
\end{aligned}$$

Rearranging the first two lines and adding and subtracting the same term $(1/3)\dot{A}(r_{31}^* + r_{32}^*)$ to the third line yields

$$\begin{aligned}
\dot{\tilde{r}}_{31} = {} & -k_1\left(r_{31} - \hat{A}r_{31}^* + r_{31} - Ar_{31}^*\right) \\
& - k_1\left(r_{32} - r_{12} + Ar_{12}^* - \hat{A}r_{32}^*\right) \\
& + \frac{1}{3}\left(\dot{\hat{A}} - \dot{A}\right)\left(r_{31}^* + r_{32}^*\right) \\
& + \frac{1}{3}\dot{A}\left(r_{31}^* + r_{32}^*\right) - \frac{1}{3}\dot{A}\left(r_{12}^* + r_{13}^*\right) - \dot{A}r_{31}^*.
\end{aligned}$$

Then, applying the same trick by adding and subtracting the term Ar_{31}^* to the first two lines of the above equation, there holds

$$\begin{aligned}
\dot{\tilde{r}}_{31} & = -k_1\left(2\tilde{r}_{31} - \left(\hat{A} - A\right)r_{31}^*\right) - k_1\left(\tilde{r}_{31} - \left(\hat{A} - A\right)r_{32}^*\right) \\
& \quad + \frac{1}{3}\left(\dot{\hat{A}} - \dot{A}\right)\left(r_{31}^* + r_{32}^*\right) + \frac{1}{3} * 3\dot{A}r_{31}^* - \dot{A}r_{31}^* \\
& = -3k_1\tilde{r}_{31} + k_1\left(\hat{A} - A\right)\left(r_{31}^* + r_{32}^*\right) + \frac{1}{3}\left(\dot{\hat{A}} - A\right) \\
& \quad \times \left(r_{31}^* + r_{32}^*\right).
\end{aligned}$$

In light of the equivalence between $(\hat{A} - A)(r_{31}^* + r_{32}^*)$ and $(\mathbf{1}_2^{\mathrm{T}} \otimes I_2)M_3^* C\tilde{v}$, we get

$$\dot{\tilde{r}}_{31} = -3k_1\tilde{r}_{31} + k_1\left(\mathbf{1}_2^{\mathrm{T}} \otimes I_2\right)M_3^* C\tilde{v} + \frac{1}{3}\left(\mathbf{1}_2^{\mathrm{T}} \otimes I_2\right)M_3^* C\dot{\tilde{v}}.$$

Recalling the fact that $\tilde{v} = T^{-1}e$, and in combination with (21), one obtains

$$\dot{\tilde{r}}_{31} = -3k_1\tilde{r}_{31} + k_1\left(\mathbf{1}_2^{\mathrm{T}} \otimes I_2\right) M_3^* C T^{-1} e + \frac{1}{3}\left(\mathbf{1}_2^{\mathrm{T}} \otimes I_2\right) M_3^* C T^{-1}\left(Fe + D\tilde{r}_3\right) \tag{32}$$

which can also be equivalently written in a relatively compact form as follows:

$$\dot{\tilde{r}}_{31} = -3k_1\tilde{r}_{31} + k_1\Psi T^{-1} e + \frac{1}{3}\Psi T^{-1}\left(Fe + D\tilde{r}_3\right).$$

REFERENCES

[1] F. Berlinger, M. Gauci, and R. Nagpal, "Implicit coordination for 3D underwater collective behaviors in a fish-inspired robot swarm," *Sci. Robot.*, vol. 6, no. 50, Jan. 2021, Art. no. eabd8668.

[2] M. Maghenem, A. Loría, E. Nuño, and E. Panteley, "Consensus-based formation control of networked nonholonomic vehicles with delayed communications," *IEEE Trans. Autom. Control*, vol. 66, no. 5, pp. 2242–2249, May 2021.

[3] M. H. Trinh, Q. V. Tran, D. V. Vu, P. D. Nguyen, and H.-S. Ahn, "Robust tracking control of bearing-constrained leader–follower formation," *Automatica*, vol. 131, Sep. 2021, Art. no. 109733.

[4] I. Buckley and M. Egerstedt, "Infinitesimal shape-similarity for characterization and control of bearing-only multirobot formations," *IEEE Trans. Robot.*, vol. 37, no. 6, pp. 1921–1935, Dec. 2021.

[5] C. Jia, F. Chen, L. Xiang, W. Lan, and G. Feng, "When distributed formation control is feasible under hard constraints on energy and time?" *Automatica*, vol. 135, Jan. 2022, Art. no. 109984.

[6] Y. Li and X. Hu, "A differential game approach to intrinsic formation control," *Automatica*, vol. 136, Feb. 2022, Art. no. 110077.

[7] Z. Lin, L. Wang, Z. Chen, M. Fu, and Z. Han, "Necessary and sufficient graphical conditions for affine formation control," *IEEE Trans. Autom. Control*, vol. 61, no. 10, pp. 2877–2891, Oct. 2016.

[8] S. Zhao, "Affine formation maneuver control of multiagent systems," *IEEE Trans. Autom. Control*, vol. 63, no. 12, pp. 4140–4155, Dec. 2018.

[9] Y. Xu, S. Zhao, D. Luo, and Y. You, "Affine formation maneuver control of high-order multi-agent systems over directed networks," *Automatica*, vol. 118, Aug. 2020, Art. no. 109004.

[10] O. Onuoha, H. Tnunay, C. Wang, and Z. Ding, "Fully distributed affine formation control of general linear systems with uncertainty," *J. Franklin Inst.*, vol. 357, no. 17, pp. 12143–12162, Nov. 2020.

[11] L. Chen, J. Mei, C. Li, and G. Ma, "Distributed leader–follower affine formation maneuver control for high-order multiagent systems," *IEEE Trans. Autom. Control*, vol. 65, no. 11, pp. 4941–4948, Nov. 2020.

[12] Y. Lin, Z. Lin, Z. Sun, and B. D. O. Anderson, "A unified approach for finite-time global stabilization of affine, rigid, and translational formation," *IEEE Trans. Autom. Control*, vol. 67, no. 4, pp. 1869–1881, Apr. 2022.

[13] H. Garcia de Marina, "Distributed formation maneuver control by manipulating the complex Laplacian," *Automatica*, vol. 132, Oct. 2021, Art. no. 109813.

[14] H. Rastgoftar and I. V. Kolmanovsky, "A spatio-temporal reference trajectory planner approach to collision-free continuum deformation coordination," *Automatica*, vol. 142, Aug. 2022, Art. no. 110255.

[15] W. Yu, B. Zhu, X. Wang, P. Yi, H. Liu, and T. Hu, "Enhanced affine formation maneuver control using historical velocity command (HVC)," *IEEE Robot. Autom. Lett.*, vol. 8, no. 11, pp. 7186–7193, Nov. 2023.

[16] Y. Rizk, M. Awad, and E. W. Tunstel, "Cooperative heterogeneous multi-robot systems: A survey," *ACM Comput. Surveys*, vol. 52, no. 2, pp. 1–31, Mar. 2020.

[17] S. Coogan and M. Arcak, "Scaling the size of a formation using relative position feedback," *Automatica*, vol. 48, no. 10, pp. 2677–2685, Oct. 2012.

[18] B.-H. Lee and H.-S. Ahn, "Distributed formation control via global orientation estimation," *Automatica*, vol. 73, pp. 125–129, Nov. 2016.

[19] Q. Yang, Z. Sun, M. Cao, H. Fang, and J. Chen, "Stress-matrix-based formation scaling control," *Automatica*, vol. 101, pp. 120–127, Mar. 2019.

[20] Q. Yang, H. Fang, M. Cao, and J. Chen, "Planar affine formation stabilization via parameter estimations," *IEEE Trans. Cybern.*, vol. 52, no. 6, pp. 5322–5332, Jun. 2022.

[21] Y. Liu, Z. Ma, F. Zhang, and P. Huang, "Time-varying formation planning and scaling control for tethered space net robot," *IEEE Trans. Aerosp. Electron. Syst.*, vol. 59, no. 5, pp. 6717–6728, Oct. 2023.

[22] K. Cao, M. Cao, and L. Xie, "Similar formation control via range and odometry measurements," *IEEE Trans. Cybern.*, vol. 54, no. 6, pp. 3765–3776, Jun. 2024.

[23] T.-M. Nguyen, Z. Qiu, T. H. Nguyen, M. Cao, and L. Xie, "Persistently excited adaptive relative localization and time-varying formation of robot swarms," *IEEE Trans. Robot.*, vol. 36, no. 2, pp. 553–560, Apr. 2020.

[24] R. Connelly and S. D. Guest, *Frameworks, Tensegrities and Symmetry: Understanding Stable Structures*. Cambridge, U.K.: Cambridge Univ. Press, 2016.

[25] Q. Yang, Z. Sun, M. Cao, H. Fang, and J. Chen, "Construction of universally rigid tensegrity frameworks and their applications in formation scaling control," in *Proc. 36th Chin. Control Conf. (CCC)*, 2017, pp. 8177–8182.

[26] F. Xiao, Q. Yang, X. Zhao, and H. Fang, "A framework for optimized topology design and leader selection in affine formation control," *IEEE Robot. Autom. Lett.*, vol. 7, no. 4, pp. 8627–8634, Oct. 2022.

[27] Z. Lin, L. Wang, Z. Chen, M. Fu, and Z. Han, "Necessary and sufficient graphical conditions necessary and sufficient graphical conditions for affine formation control," *IEEE Trans. Autom. Control*, vol. 61, no. 10, pp. 2877–2891, Oct. 2016.

[28] M. Mesbahi and M. Egerstedt, "Graph theoretic methods in multiagent networks," in *Graph Theoretic Methods in Multiagent Networks*. Princeton, NJ, USA: Princeton Univ. Press, 2010.

[29] Q. Yang, Z. Sun, M. Cao, H. Fang, and J. Chen, "Construction of universally rigid frameworks and their applications in formation scaling control," in *Proc. 36th Chin. Control Conf.*, 2017, pp. 163–168.

[30] B. Datta, *Numerical Methods for Linear Control Systems*, vol. 1. Cambridge, MA, USA: Academic Press, 2004.

[31] R. A. Horn and C. R. Johnson, *Matrix Analysis*. Cambridge, U.K.: Cambridge Univ. Press, 2012.

[32] K. Fathian, S. Safaoui, T. H. Summers, and N. R. Gans, "Robust distributed planar formation control for higher order holonomic and nonholonomic agents," *IEEE Trans. Robot.*, vol. 37, no. 1, pp. 185–205, Feb. 2021.

[33] P. C. Lusk, X. Cai, S. Wadhwania, A. Paris, K. Fathian, and J. P. How, "A distributed pipeline for scalable, deconflicted formation flying," *IEEE Robot. Autom. Lett.*, vol. 5, no. 4, pp. 5213–5220, Oct. 2020.

[34] Z. Wen, D. Goldfarb, and W. Yin, "Alternating direction augmented Lagrangian methods for semidefinite programming," *Math. Program. Comput.*, vol. 2, nos. 3–4, pp. 203–230, Dec. 2010.

[35] J. A. Preiss, W. Hönig, G. S. Sukhatme, and N. Ayanian, "Crazyswarm: A large nano-quadcopter swarm," in *Proc. IEEE Int. Conf. Robot. Autom. (ICRA)*, May 2017, pp. 3299–3304.

[36] *Crazyswarm*. Accessed: Aug. 29, 2024. [Online]. Available: https://github.com/USC-ACTLab/crazyswarm

[37] *API Reference of Crazyswarm*. Accessed: Aug. 29, 2024. [Online]. Available: https://crazyswarm.readthedocs.io/en/latest/api.html

Qingkai Yang (Member, IEEE) received the first Ph.D. degree in control science and engineering from Beijing Institute of Technology, Beijing, China, in 2018, and the second Ph.D. degree in system control from the University of Groningen, Groningen, The Netherlands, in 2018.

He is currently a Professor with the School of Automation, Beijing Institute of Technology. His research interests include the cooperative control of multiagent systems, autonomous mobile robots, and swarm intelligence.

Xiaozhen Zhang received the M.S. degree in navigation, guidance and control from Northwestern Polytechnical University, Xi'an, China, in 2021. He is currently pursuing the Ph.D. degree in control engineering with Beijing Institute of Technology, Beijing, China.

His research interests include swarm robotics, multiagent systems, and distributed control.

Hao Fang (Member, IEEE) received the B.S. degree from Xi'an University of Technology, Xi'an, Shaanxi, China, in 1995, and the M.S. and Ph.D. degrees from Xi'an Jiaotong University, Xi'an, in 1998 and 2002, respectively.

He held two post-doctoral appointments at the INRIA/France Research Group of COPRIN, Paris, France, and LASMEA, UNR6602 CNRS/Blaise Pascal University, Clermont-Ferrand, France. Since 2011, he has been a Professor with Beijing Institute of Technology, Beijing, China. His research interests include all-terrain mobile robots, robotic control, and multiagent systems.

Ming Cao (Fellow, IEEE) received the bachelor's and master's degrees from Tsinghua University, Beijing, China, in 1999 and 2002, respectively, and the Ph.D. degree from Yale University, New Haven, CT, USA, in 2007.

He joined the IBM T. J. Watson Research Center, Yorktown Heights, NY, USA, as a Research Intern, in 2006. From 2007 to 2008, he was a Research Associate with Princeton University, Princeton, NJ, USA. He joined the Engineering and Technology Institute (ENTEG), University of Groningen, Groningen, The Netherlands, as an Assistant Professor, in 2008, where he has been a Professor of networks and robotics since 2016 and the Director of the Jantina Tammes School of Digital Society, Technology and AI, since 2022. His research interests include autonomous robots and multiagent systems, complex networks, and decision-making processes.

Dr. Cao was a recipient of Manfred Thoma Medal from the International Federation of Automatic Control (IFAC) in 2017 and European Control Award sponsored by the European Control Association (EUCA) in 2016. He is a Senior Editor of *Systems and Control Letters* and an Associate Editor of IEEE TRANSACTIONS ON AUTOMATIC CONTROL, IEEE TRANSACTIONS OF CONTROL OF NETWORK SYSTEMS, and IEEE ROBOTICS & AUTOMATION MAGAZINE, and was an Associate Editor of IEEE TRANSACTIONS ON CIRCUITS AND SYSTEMS I: REGULAR PAPERS and *IEEE Circuits and Systems Magazine*. He is a member of the IFAC Council.

Jie Chen (Fellow, IEEE) received the B.Sc., M.Sc., and Ph.D. degrees in control theory and control engineering from Beijing Institute of Technology, Beijing, China, in 1986, 1996, and 2001, respectively.

He was the President of Tongji University, Shanghai, China, from 2018 to 2023. He is currently a Professor of control science and engineering with Beijing Institute of Technology and Tongji University, where he serves as the Director of the National Key Laboratory of Autonomous Intelligent Unmanned Systems (KAIUS). His research interests include complex systems, multiagent systems, multiobjective optimization and decision, and constrained nonlinear control.

Prof. Chen is currently the Editor-in-Chief of *Unmanned Systems* and the *Journal of Systems Science and Complexity*. He has served on the editorial boards of several journals, including IEEE TRANSACTIONS ON CYBERNETICS, *International Journal of Robust and Nonlinear Control*, and *Science China Information Sciences*. He is a fellow of IFAC and a member of the Chinese Academy of Engineering.